Synthesis and Redox Characterization of the Polyoxo Anion, γ*-$[S_2W_{18}O_{62}]^{4-}$: A Unique Fast Oxidation Pathway Determines the Characteristic Reversible Electrochemical Behavior of Polyoxometalate Anions in Acidic Media

Peter J. S. Richardt,[†] Robert W. Gable,[†] Alan M. Bond,[‡] and Anthony G. Wedd*[,†]

School of Chemistry, University of Melbourne, Parkville, Victoria 3052, Australia, and Department of Chemistry, Monash University, Clayton, Victoria 3168, Australia

Received July 17, 2000

The synthesis and characterization of $(Bu_4N)_4[S_2W_{18}O_{62}]\cdot 1.23MeCN\cdot 0.27H_2O$ are reported. It crystallizes in the monoclinic space group *C*2/*c* with $a = 22.389(6)$ Å, $b = 22.104(3)$ Å, $c = 25.505(5)$ Å, $\beta = 95.690(15)°$, $V = 12560(5)$ Å^3, and $Z = 4$. The anion exists as the γ* isomer, the second example of this isomer type to be characterized structurally. The equivalent molybdenum salt occurs as the α isomer. γ*-$[S_2W_{18}O_{62}]^{4-}$ in MeCN solution displayed four electrochemically reversible one-electron redox processes at $E_{1/2}$ values of −0.24, −0.62, −1.18, and −1.57 V versus the Fc^+/Fc couple. Upon addition of acid in MeCN/H_2O (95/5 v/v), the two most cathodic processes converted to an overall two-electron process at −0.71 V. The total data suggested that this process actually comprises two one-electron transfer processes, occurring at different potentials, with associated proton-transfer reactions. The interpretation is supported by simulation of the effect of acid titration upon the cyclic voltammetry. While multiple pathways for correlated reduction and protonation are present in both the molybdenum and tungsten systems, only a single fast oxidation pathway is available. As the reduced forms of $[S_2W_{18}O_{62}]^{4-}$ are much weaker bases than those of $[S_2Mo_{18}O_{62}]^{4-}$, the individual oxidation pathways are not the same. However, their existence determines the highly reversible electrochemical behavior that is characteristic of these anions, and that of polyoxometalate systems in general.

Introduction[1]

The structure of the classic polyoxo anions of stoichiometry $[X_2M_{18}O_{62}]^{n-}$ was defined initially by Dawson for α-$[P_2W_{18}O_{62}]^{6-}$.[2] The α isomer exhibits nominal D_{3h} point symmetry (structure I).[3] A number of other isomers, differing in the relative orientations of the trinuclear "caps" or hexanuclear "belts",[4,5] have been defined by X-ray crystallography,[2,6−10] or have been proposed to exist in solution on the basis of NMR data.[5,11,12] In particular, the γ* isomer (structure II, D_{3d}) is derived formally from the α form by 60° rotation of one-half of the ion relative to the other, followed by 60° rotations of both trinuclear caps.

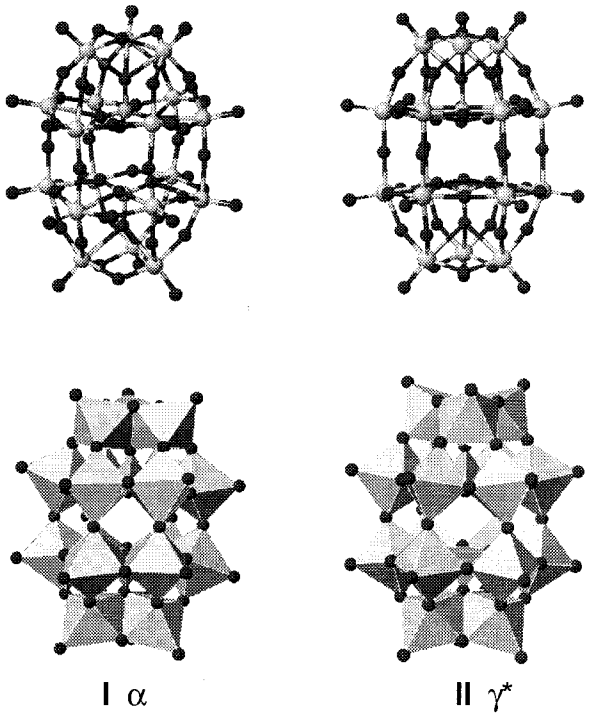

The present work reports the synthesis and structural characterization of γ*-$(Bu_4N)_4[S_2W_{18}O_{62}]$, the second γ* isomer to be characterized structurally. Its synthesis arose from a desire to compare its redox and photochemical properties with those

* t.wedd@chemistry.unimelb.edu.au.
[†] University of Melbourne.
[‡] Monash University.

(1) Abbreviations: a, anodic; Bu, *n*-butyl; c, cathodic; CV, cyclic voltammetry; D_f, diffusion coefficient; *E*, potential; $E_{1/2}$, reversible half-wave potential; ΔE_p, difference between peak potentials; ESI-MS, electrospray ionization mass spectrometry; *F*, Faraday's constant; Fc, ferrocene; *i*, current; i_L, limiting current; i_p, peak current; m, medium; M, molar concentration; *n*, number of electrons transferred per mole; N_r, rotation rate (min^{-1}); RDEV, rotating disk electrode voltammetry; sh, shoulder; *T*, temperature; *v*, scan rate; w, weak; ω, rotation rate (s^{-1}).

(2) Dawson, B. *Acta Crystallogr.* **1953**, *6*, 113.
(3) Pope, M. T. *Heteropoly and Isopoly Oxometalates*; Springer-Verlag: Berlin, 1983; pp 69−70.
(4) Baker, L. C. W.; Figgis, J. S. *J. Am. Chem. Soc.* **1970**, *92*, 3794.
(5) Contant, R.; Thouvenot, R. *Inorg. Chim. Acta* **1993**, *212*, 41.
(6) Strandberg, R. *Acta Chem. Scand., Ser. A* **1975**, *29*, 350.
(7) D'Amour, H. *Acta Crystallogr.* **1976**, *B32*, 729.
(8) Wéry, A. S. J.; Gutiérrez-Zorrilla, J. M.; Luque, A.; Ugalde, M.; Román, P. *Polyhedron* **1997**, *16*, 2589.
(9) Neubert, H.; Fuchs, J. *Z. Naturforsch. Teil B* **1987**, *42*, 951.
(10) Hori, T.; Tamada, O.; Himeno, S. *J. Chem. Soc., Dalton Trans.* **1989**, 1491.
(11) Massart, R.; Contant, R.; Fruchart, J.-M.; Ciabrini, J.-P.; Fournier, M. *Inorg. Chem.* **1977**, *16*, 2916.
(12) Acerete, R.; Harmalker, S.; Hammer, C. F.; Pope, M. T.; Baker, L. C. W. *J. Chem. Soc., Chem. Commun.* **1979**, 777.

10.1021/ic000793q CCC: $20.00
Published on Web 01/11/2001

of the intensively studied α-$[S_2Mo_{18}O_{62}]^{4-}$ ion.[10,13−21] For the latter, an extensive series of reduction processes (addition of up to 26 electrons in acid media) has been identified.[17] The reduced anions are basic, and simulation of experimental data has unravelled many aspects of the coupling of electron and proton transfer in these systems.[18,20] These insights led to the directed synthesis of various reduced forms of α-$[S_2Mo_{18}O_{62}]^{4-}$ in a number of different protonation states.[18]

A detailed comparison of the electrochemical properties of the Mo and W systems in aprotic and protic media is presented here. The reduced forms of $[S_2W_{18}O_{62}]^{4-}$ are much weaker bases than those of $[S_2Mo_{18}O_{62}]^{4-}$. However, in each system, while multiple reduction/protonation pathways are possible in the presence of acidic electrolyte media, only a single fast oxidation pathway is available. This determines the highly reversible electrochemical behavior characteristic of polyoxometalate anions in protic media.

Experimental Section

Reagents. $Na_2WO_4 \cdot 2H_2O$ and $Na_2MoO_4 \cdot 2H_2O$ were reagent grade chemicals from APS Ajax Finechem. CH_3CN, Et_2O, and EtOH were analytical grade chemicals from APS Ajax Finechem. Bu_4NBr was purchased from the Aldrich Chemical Co. Inc., Milwaukee, WI.

Synthesis. $[Bu_4N]_4[S_2W_{18}O_{62}] \cdot 1.23MeCN \cdot 0.27H_2O$. $Na_2WO_4 \cdot 2H_2O$ (50 g, 0.15 mol) was dissolved in a boiling solution of CH_3CN (175 cm^3) and H_2O (175 cm^3). H_2SO_4 (9 M, 75 cm^3) was added dropwise to the refluxing solution with vigorous stirring. The resulting light yellow mixture was refluxed for 16 h and was then allowed to cool to room temperature. The mixture separated into two phases, a light yellow upper phase and a slightly cloudy, colorless lower phase. The upper phase was collected, and the crude product was precipitated by addition of solid Bu_4NBr (10.9 g, 0.03 mol) in small portions with vigorous stirring. The resulting waxy solid was left in the freezer for several hours to solidify before filtration. It was washed with EtOH and Et_2O and dried under vacuum. Fractional recrystallization from hot MeCN produced analytically pure material by the second crop. Yield: 12.4 g, 28%. IR: ν(WOS), 1180, m; 1075, w; ν(W=O), 965, s; ν(WOW), 905, m, 805, s. UV−vis: λ_{max}, nm (ϵ, M^{-1} cm^{-1}), 252 (5.75×10^4); 300 sh (3.93×10^4). Anal. Found: C, 14.68; H, 2.59; N, 1.19; S, 1.14; W, 62.45%. Atom ratios are N:S:W = 4.5:1.9:18. $C_{64}H_{144}N_4O_{62}S_2W_{18}$ requires C, 14.41; H, 2.72; N, 1.05; S, 1.20; W, 62.03%. The high experimental N:W ratio suggests the presence of CH_3CN of crystallization, consistent with the X-ray diffraction data (see below). For 0.5 equiv of CH_3CN of crystallization, $C_{65}H_{145.5}N_{4.5}O_{62}S_2W_{18}$ requires C, 14.58; H, 2.74; N, 1.18; S, 1.20; W, 61.79%. For one CH_3CN of crystallization, $C_{66}H_{147}N_5O_{62}S_2W_{18}$ requires C, 14.75; H, 2.76; N, 1.30; S, 1.19; W, 61.55%.

Instrumental Techniques. Elemental analysis was performed at the Analytische Laboratorien, Elbach, Germany. Electronic spectra were recorded on a Cary 1C UV−visible spectrophotometer. Data collection employed a generic 486 PC, running Cary version 2.50 software, on an OS/2 WARP version 3 operating platform. The spectrophotometric cells were quartz with a 1 cm path length. Infrared spectra of pressed KBr disks were recorded on a Bio-Rad FTS-165 Fourier Transform spectrometer.

Electrochemistry. Voltammograms were obtained using a Cypress Systems model CS1087E electroanalysis system. The standard three-electrode arrangement was employed with a Pt wire auxiliary electrode, glassy carbon working electrode, and Ag/AgCl (saturated NaCl in MeCN) reference electrode, for both rotating-disk voltammetry and cyclic voltammetry. The reference electrode was calibrated against the ferricenium/ferrocene (Fc^+/ Fc) couple. All potentials are quoted relative to this standard. The glassy carbon working electrodes (diameter 2.8 mm) were polished with alumina (3 μm) on LECO Inc. polishing pads and then rinsed with distilled water and dried before each experiment. The cell was purged with N_2 for at least 10 min before each experiment. Rotating disk voltammetric measurement was undertaken with a Metrohm 2.8 mm diameter glassy carbon working electrode, which was rotated by a variable speed Metrohm 628-10 rotator.

Simulation of Cyclic Voltammograms. The simulation package DIGISIM V 2.0 (Bioanalytical Systems, West Lafayette, IN) is described in ref 22. A systematic approach to simulation of the complex voltammetry of polyoxometalate anions as a function of pH has been developed and was employed here.[20] A 150 MHz Pentium PC was employed, and each simulation required about 5 s. A number of background input parameters are defined here via goodness of fit estimates for voltammograms in MeCN. Uncompensated resistance: 400 Ω.. Double layer capacitance: 2×10^{-6} F. Temperature: 298 K. Electrode area: estimated experimentally as 0.075 cm^2 via application of the Levich equation[23a] to RDEV data for the Fc^+/Fc couple; simulations were optimized at a value of 0.08 cm^2, and this was the value used in the final simulations. Charge-transfer coefficients: 0.5; this parameter did not affect the simulations, consistent with the presence of electrochemically reversible processes. Heterogeneous charge-transfer rate constants: assumed to be fast, and set at 1 cm s^{-1}. Diffusion coefficients (D_f) for $[S_2W_{18}O_{62}]^{n-}$ ($n = 4-8$): these were estimated experimentally for $n = 4-6$ as $4.4(3) \times 10^{-6}$, $3.7(1) \times 10^{-6}$, and $3.8(1) \times 10^{-6}$ cm^2 s^{-1}, respectively, via application of the Levich equation[23a] to RDEV data in MeCN;[24] however, $D_f = 4.4 \times 10^{-6}$ cm^2 s^{-1} was used for each species, as the simulations were not sensitive to the variations detected experimentally. The diffusion coefficient for H^+ was optimized to a final value of 1.5×10^{-5} cm^2 s^{-1} in the fitting process.[20]

Crystal Data. Single crystals were grown by dissolution of $[Bu_4N]_4[S_2W_{18}O_{62}]$ (5×10^{-3} M) in MeCN (0.1 M Bu_4NClO_4) at room temperature followed by standing at 4 °C. As crystals rapidly lost solvent when exposed to the atmosphere, data were collected on a crystal mounted in a Lindemann glass-capillary tube, in the presence of mother liquor. In addition, many of the crystals were found to be disordered, with broad and asymmetric peaks; the selected crystal (0.15 × 0.14 × 0.08 mm) showed comparitively little disorder. Intensity data were collected (h, −1 to +26; k, −1 to +26; l, −30 to +30) using an Enraf-Nonius CAD-4MachS single-crystal X-ray diffractometer and the ω:2θ scan method, with Mo Kα radiation (graphite crystal monochromator), $\lambda = 0.71073$ Å, at 293(1) K. The data were corrected for absorption by Gaussian integrations (SHELX76); maximum and minimum transmission coeficients were 0.389 and 0.142. Accurate values of the unit-cell parameters and crystal orientation were obtained by a least-squares procedure from the angular settings of 25 carefully centered reflections. The crystal showed a deterioration of 10% during the data collection. A total of 12 656 reflections were collected, of which 191 were omitted due to obviously high or asymmetric backgrounds, and 10 991 were unique and subsequently used in the refinement ($R_{int} = 0.053$); of these 7249 had $I > 2\sigma(I)$. Crystallographic data are summarized in Table 1 and are available as a CIF file.

Structure Solution and Refinement. The structure was solved from a combination of direct methods and difference syntheses[25,26] and was refined using a full-matrix least-squares refinement procedure on

(13) Hori, T.; Himeno, S. *Chem. Lett.* **1987**, 53.
(14) Himeno, S.; Hori, T.; Saito, A. *Bull. Chem. Soc. Jpn.* **1989**, *62*, 2184.
(15) Cooper, J. B.; Way, D. M.; Bond, A. M.; Wedd, A. G. *Inorg. Chem.* **1993**, *32*, 2416.
(16) Bond, A. M.; Way, D. M.; Wedd, A. G.; Compton, R. G.; Booth, J.; Eklund, J. C. *Inorg. Chem.* **1995**, *34*, 3378.
(17) Way, D. M.; Bond, A. M.; Wedd, A. G. *Inorg. Chem.* **1997**, *36*, 2826.
(18) Way, D. M.; Cooper, J. B.; Sadek, M.; Vu, T.; Mahon, P. J.; Bond, A. M.; Brownlee, R. T. C.; Wedd, A. G. *Inorg. Chem.* **1997**, *36*, 4227; **1998**, *37*, 604 (erratum).
(19) Bond, A. M.; Ecklund, J. C.; Tedesco, V.; Vu, T.; Wedd, A. G. *Inorg. Chem.* **1998**, *37*, 2366.
(20) Prenzler, P. D.; Boskovic, C.; Bond, A. M.; Wedd, A. G. *Anal. Chem.* **1999**, *71*, 3650.
(21) Eklund, J. C.; Bond, A. M.; Humphry, D. G.; Lazarev, G.; Vu, T.; Wedd, A. G.; Wolfbauer, G. *J. Chem. Soc., Dalton Trans.* **2000**, 4373.
(22) Rudolph, M.; Reddy, D. P.; Feldberg, S. W. *Anal. Chem.* **1994**, *66*, 589A.
(23) Bard, A. J.; Faulkner, L. R. *Electrochemical Methods, Fundamentals and Applications*; Wiley: New York, 1980; (a) p 288. (b) p 229. (c) pp 160, 290.
(24) Richardt, P. J. S. Ph.D. thesis, University of Melbourne, 2000.
(25) Sheldrick, G. M., SHELXS-97. Program for Crystal Structure Solution, University of Gottingen, Germany, 1997.

Table 1. Crystallographic Data for γ^*-$[Bu_4N]_4[S_2W_{18}O_{62}]\cdot 1.23MeCN\cdot 0.27H_2O$

formula	C66.46 H146.23 N5.23 O62.27 S2 W18
fw	5445.97
a,Å	22.389(6)
b, Å	22.104(3)
c, Å	25.505(5)
β, deg	95.690(15)
V, Å^3	12560(5)
Z	4
space group	*C*2/*c*
ρ, cm^{-1}	2.880
μ, cm^{-1}	16.53
scan method	$\omega/2\theta$
data	12456
unique data	10991
$2\theta_{max}$, deg	50
weight (*w*)	$[\sigma^2(F_o^2) + (0.0886P)^2 + 0P]^{-1}$
data refined	10991
R^a	0.0552
R_w ^{b}	0.1483
max shift/esd	0.003
max, min diff peak, $\times 10^{-3}$ Å	1.90, −2.63

^{a} $R = \sum||F_o| - |F_c||/\sum F_o$. ^{b} $Rw = [\sum w(F_o^2 - F_c^2)^2/\sum w(F_o^2)^2]^{1/2}$.

F^2. Anisotropic displacement parameters were assigned to all non-H atoms; no hydrogen atoms were located. The anion lies on a center of symmetry (1/4, 1/4, 0), while the two unique cations are in general positions. The anion was found to be disordered, with two minor components that were able to be included in the refinement, these being translated by approximately ±(0.35, 0, −0.27), with respect to the major component. All atoms in these components were assigned a common isotropic displacement parameter, and the geometrical parameters were restrained to be similar to that of the major component. The final occupancy factors were 0.934(3):0.033(2):0.033(2). The cations were also disordered, with the two terminal carbon atoms in every NC_4 chain distributed over two positions and being given isotropic displacement parameters; all of these disordered atoms were restrained to ideal geometry. One molecule of MeCN (restrained to ideal geometry) was located lying along a two-fold axis, while another solvent site appeared to be a combination of MeCN (atoms in fixed positions) and water. For the latter solvent site, while the relative amounts were allowed to vary, the sum of the MeCN and water was fixed at one molecule. There was no evidence for the presence of other solvent molecules, which suggested that if there was additional solvent it was essentially fluid in nature. The final refined proportions of solvent molecules were 1.23 MeCN and 0.27 water. All solvent atoms were given a fixed isotropic displacement parameter. The refinement converged with R [$I > 2\sigma(I)$] and R_w (all data) of 0.0552 and 0.1483, respectively. The weighting scheme employed was of the type $w = [s^2(F_o^2) + (0.0886P)^2 + 0P]^{-1}$. In the final difference map, maximum and minimum peak heights were $+1.90 \times 10^{-3}$ and -2.63×10^{-3}Å, close to the W atoms of the anion, and represent components of the disorder that were not modeled. The molecular structure of the anion is shown in Figure 1, while selected interatomic distances and angles are included in Table 2.

Results and Discussion

Synthesis. Detailed investigations of $Na_2MoO_4\cdot 2H_2O$ and H_2SO_4 in MeCN/H_2O showed that the yield of the α-$[S_2Mo_{18}O_{62}]^{4-}$ ion was optimized for MeCN/H_2O > 3/2 and $[H_2SO_4]/[Mo] > 4/1$.[14] The lower solubility of $Na_2WO_4\cdot 2H_2O$ meant that MeCN/H_2O = 1/1 was used in the present system, with $[H_2SO_4]/[W] = 4.7/1$. Reflux of the mixture yielded a two-phase system. Addition of Bu_4NBr to the MeCN-rich layer provided a mixture of salts of $[W_6O_{19}]^{2-}$ and $[S_2W_{18}O_{62}]^{4-}$. Fractional recrystallization from MeCN proved to be the most effective separation technique. Two recrystallizations provided pure material, as judged by microanalysis and ESI-MS.

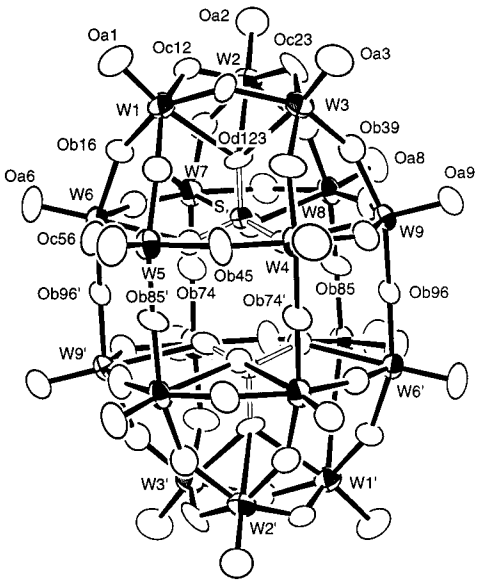

Figure 1. Molecular structure and labeling scheme of the anion in $[Bu_4N]_4[S_2W_{18}O_{62}]\cdot 1.23MeCN\cdot 0.27H_2O$. Primed atoms are related to the unprimed atoms by the symmetry operator $1/2 - x$, $1/2 - y$, $-z$. Ellipsoids are at the 50% probability level.

Molecular Structure. The $[S_2W_{18}O_{62}]^{4-}$ anion in $[Bu_4N]_4[S_2W_{18}O_{62}]\cdot 1.23MeCN\cdot 0.27H_2O$ is the γ^* isomer (structure II; Figure 1) rather than the α isomer (structure I) that is observed in $[Bu_4N]_4[S_2Mo_{18}O_{62}]\cdot MeCN$.[10] A γ^* isomer has been characterized structurally in one other system, $[NH_4]_6[As_2W_{18}O_{62}]$, and an α form of this salt is also known.[9] Table S1 is a full listing of interatomic distance and angle data for the four anions mentioned above. Tables 2 and 3 list minimal comparitive structural parameters only. Assuming the radii of Mo and W to be similar,[27] bond length differences can be attributed to the smaller effective size of the SO_4 unit relative to AsO_4. For example, the M−OS distances (M−O_{d123}; M = Mo, W) are 0.1−0.2 Å longer than W−OAs distances (Table 2).

Contant and Thouvenot discussed the relative stabilities of the α and γ^* isomers, emphasising the structural influence of the eclipsed junction between the hexanuclear belts in the α form (D_{3h}; structure I) relative to that of the staggered junction in the γ^* form (D_{3d}; structure II).[5] Figure 2 details the O···O nonbonded separations within the belts for the α-$[S_2Mo_{18}O_{62}]^{4-}$ and γ^*-$[S_2W_{18}O_{62}]^{4-}$ anions. The upper hexagons of bridging O atoms (Ob16), which link the belts with the caps, each feature alternating shorter and longer nonbonding separations. On the other hand, the lower hexagons of bridging O atoms (Ob96), which link the two halves of the molecules (Figure 1), have similar separations in the γ^* isomer, but alternating shorter and longer separations in the α isomer (Figure 2; Table 3). The smaller effective size of the SO_4 unit is consistent with the smaller average separation of these O_b atoms (3.63 Å) within the larger hexagon in γ^*-$[S_2W_{18}O_{62}]^{4-}$, relative to that of 3.75 Å in γ^*-$[As_2W_{18}O_{62}]^{4-}$. In addition, the relative orientations of the six individual octahedra within the belt adjust to accommodate the different sizes of the S and As atoms. The W−Ob96−W links between the belts are effectively linear (average angle, 179°; Table 2) in γ^*-$[S_2W_{18}O_{62}]^{4-}$ compared to 168° in γ^*-$[As_2W_{18}O_{62}]^{4-}$.

(26) Sheldrick, G. M., SHELXL-97. Program for Crystal Structure Refinement, University of Gottingen, Germany, 1997.

(27) Huhey, J. E.; Keiter, E. A.; Keiter, R. L. *Inorganic Chemistry*, 4th ed.; Harper-Collins: New York, 1993; pp 114−117.

Table 2. Mean Interatomic Distances (Å), Bond Angles (Deg), and Observed Ranges[a] in α-$[Bu_4N]_4[S_2Mo_{18}O_{62}]$, γ*-$[Bu_4N]_4[S_2W_{18}O_{62}]$, and α- and γ*-$[H_4N]_6[As_2W_{18}O_{62}]$

	α-$[S_2Mo_{18}O_{62}]^{4-}$ [b]	γ*-$[S_2W_{18}O_{62}]^{4-}$ [c,d]	γ*-$[As_2W_{1'8}O_{62}]^{6-}$ [e]	α-$[As_2W_{1'8}O_{62}]^{6-}$ [e]
M−O (Od56)	2.47 ± 0.04	2.53 ± 0.04	2.37 ± 0.08	2.30 ± 0.05
M−O (Od123)	2.50 ± 0.06	2.53 ± 0.02	2.41 ± 0.02	2.32 ± 0.03
X−O (Od56)[f]	1.46 ± 0.04	1.46 ± 0.01	1.67 ± 0.06	1.69 ± 0.03
X−O (Od123)[f]	1.48 ± 0.04	1.48 ± 0.01	1.57 ± 0.01	1.74 ± 0.01
X···X[f]	3.92	3.774	3.86	3.85
Od56−M−Oa6	170 ± 2	171 ± 2	166 ± 7	171 ± 4
M−Ob45−M	153 ± 2	161 ± 1	155 ± 8	154 ± 3
M−Ob96−M	164 ± 1	179 ± 1	168 ± 2	161 ± 1
M−Oc12−M	128 ± 2	132 ± 2	126 ± 3	122 ± 2
M−Oc56−M	129 ± 3	131 ± 1	133 ± 6	121 ± 2
M−Od56−M	89 ± 2	87 ± 1	94 ± 2	94 ± 2

[a] Key to labeling of specific oxygen atoms is given in Figure 1. The observed values for all symmetry equivalent parameters are indicated as a ± range. [b] Reference 10. [c] This work. [d] Typical esd values (Å or °) for γ*-$[Bu_4N]_4[S_2W_{18}O_{62}]\cdot 1.23MeCN\cdot 0.27H_2O$ are W−O, 0.01; S−O, 0.01; S···S, 0.008; OWO, 0.6; WOW, 0.6; WOS, 0.6. [e] Reference 9. [f] X = S or As.

Table 3. Observed Ranges of O···O Distances (Å)[a] in α-$[Bu_4N]_4[S_2Mo_{18}O_{62}]$, γ*-$[Bu_4N]_4[S_2W_{18}O_{62}]$, and α- and γ*-$[H_4N]_6[As_2W_{18}O_{62}]$

hexagon	corner (c)- or edge (e)-shared octahedra	α-$[S_2Mo_{18}O_{62}]^{4-}$	γ*-$[S_2W_{18}O_{62}]^{4-}$ [c]	γ*-$[As_2W_{18}O_{62}]^{6-}$	α-$[As_2W_{18}O_{62}]^{6-}$
lower[b]	c	4.18 ± 0.04			4.34 ± 0.01
	c and e		3.63 ± 0.01	3.75 ± 0.05	
	e	3.08 ± 0.03			3.13 ± 0.01
upper[b]	c	2.58 ± 0.01	3.29 ± 0.04	3.24 ± 0.02	2.62 ± 0.02
	e	3.17 ± 0.04	2.53 ± 0.03	2.55 ± 0.04	3.05 ± 0.05

[a] The observed values are indicated as a ± range. Data taken from references footnoted in Table 2. [b] See Figure 2. [c] Esd values for O···O distances in this anion are typically 0.02 Å.

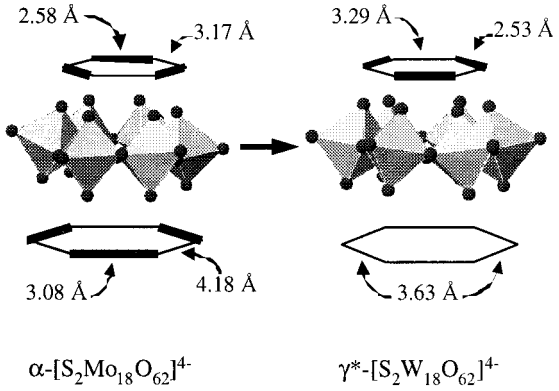

Figure 2. Representation of O···O nonbonded separations in the α-$[S_2Mo_{18}O_{62}]^{4-}$ and γ*-$[S_2W_{18}O_{62}]^{4-}$ anions. A polyhedral representation of one of the hexanuclear belts is shown. The upper hexagon represents the bridging atoms O_b which link a belt with a cap. The lower hexagon represents the bridging atoms O_b which link belts. A thicker line indicates a smaller O···O separation. Average interatomic distances are indicated.

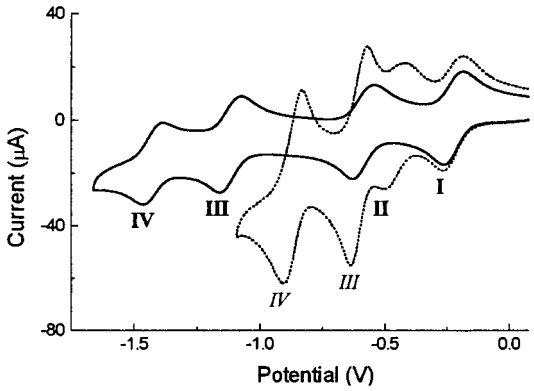

Figure 3. Cyclic voltammograms of $[Bu_4N]_4[S_2W_{18}O_{62}]$ (1.0×10^{-3} M) in MeCN/H_2O (95/5, v/v; 0.1 M Bu_4NClO_4); ν, 0.100 V s^{-1}. No added acid (—); plus four mole equivalents of $HClO_4$ (- - -).

Electrochemistry in MeCN. A cyclic voltammogram for a solution of $[Bu_4N]_4[S_2W_{18}O_{62}]$ (1.0×10^{-3} M) in MeCN, with Bu_4NClO_4 (0.1 M) as supporting electrolyte, is shown in Figure S4. Four major reduction processes **I**−**IV** are present in the region 0 to −1.8 V (cf, Figure 3). Less well-defined processes were observed at more negative potentials.

The $E_{1/2}$ value, the current function $i_{pc}\nu^{1/2}$, and current ratio $|i_{pa}/i_{pc}|$ for process **I** are independent of scan rate within experimental error (Table S2). ΔE_p increased from 0.060 to 0.090 V in the scan-rate range ν, 0.020−1.0 V s^{-1}. A constant value of $\Delta E_p = 0.057/n$ V is expected for an electrochemically reversible process involving transfer of n electron equivalents.[23b] Comparison of the data for process **I** with those for the Fc^+/Fc redox couple (known to undergo rapid and reversible electrochemical equilibrium at the electrode[28,29]) confirms process **I** as a reversible $1e^-$ transfer. The slight dependence of ΔE_p on scan rate is attributable to uncompensated resistance in the electrochemical cell rather than to slow electron transfer.

Scheme 1

$$[S_2W_{18}O_{62}]^{4-} \underset{\mathbf{I}}{\overset{e^-}{\rightleftharpoons}} [S_2W_{18}O_{62}]^{5-} \underset{\mathbf{II}}{\overset{e^-}{\rightleftharpoons}} [S_2W_{18}O_{62}]^{6-} \underset{\mathbf{III}}{\overset{e^-}{\rightleftharpoons}} [S_2W_{18}O_{62}]^{7-} \underset{\mathbf{IV}}{\overset{e^-}{\rightleftharpoons}} [S_2W_{18}O_{62}]^{8-}$$

Examination of the data for processes **II**−**IV** (Table S2) indicates that each is essentially reversible. The voltammetry is consistent with $[S_2W_{18}O_{62}]^{4-}$ undergoing four consecutive reduction processes, **I**−**IV**, each of which involves transfer of $1e^-$ on the voltammetric time scale (Scheme 1).

This conclusion is supported by the simulation displayed in Figure S4, using $E_{1/2}$ values estimated from Table S2. A

(28) Sawyer, D. T.; Sobkowiak, A.; Roberts, J. L., Jr. *Electrochemistry for Chemists*, 2nd ed.; Wiley: New York, 1995; p 203.
(29) Gritzner, G.; Kuta, J. *Pure Appl. Chem.* **1984**, *56*, 461.

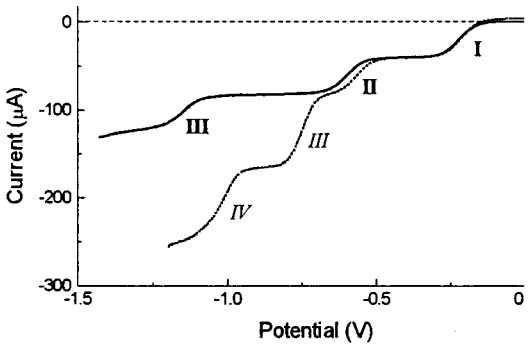

Figure 4. Rotating disk electrode voltammograms of $[Bu_4N]_4[S_2W_{18}O_{62}]$ (1.0×10^{-3} M) in MeCN/H_2O (95/5, v/v; 0.1 M Bu_4NClO_4; ν, 0.010 V s^{-1}). N_r, 2000 min^{-1}. No added acid (—); plus four mole equivalents of $HClO_4$ (- - -).

resistance term of 400 Ω was needed to account for the uncompensated resistance discussed above. There is a mismatch in baseline for processes **III** and **IV** which is attributed to nonlinear dependence of the background current and/or to the influence of the processes at more negative potentials.

Well-resolved waves were observed for processes **I** and **II** in rotating disk voltammograms under the same conditions (Figure S5; cf. Figure 4). Processes **III** and **IV** were not observable, consistent with the product of process **II** adsorbing or precipitating and subsequently blocking the electrode surface at the higher current densities associated with RDEV.[30] The position of zero current confirmed the presence of fully oxidized $[S_2W_{18}O_{62}]^{4-}$ in solution. $E_{1/2}$ values for processes **I** and **II** were essentially independent of rotation rate (Table S3), and plots of the Levich equation (i_L vs $\omega^{1/2}$)[23a] for processes **I** and **II** are linear (Figure S6), consistent with a mass-transport-controlled reversible process. Plots of E versus $\ln[(i_L - i)/i]$[23c] are also linear (Figure S6), and estimates of n (n_{app}; Table S3), obtained from the slopes, are consistent with $1e^-$ processes.[31] The results confirm the conclusions derived from the cyclic voltammetry (Scheme 1).

Electrochemistry in MeCN/H_2O. Cyclic voltammograms in MeCN/H_2O (95/5 v/v; Bu_4NClO_4, 0.1 M) also showed processes **I**−**IV** (Figure 3). $E_{1/2}$ values were displaced in the positive direction by 0.2−0.14 V, symptomatic of Nernstian shifts in potential induced by a medium effect.[17] RDEV detects processes **I**−**III** (Figure 4); the presence of water apparently suppresses interactions of the product of process **II**, $[S_2W_{18}O_{62}]^{6-}$, at the electrode surface (cf. Figure S5). The relative magnitudes of the limiting currents (1:0.95:0.9; N_r, 2000 min^{-1}), combined with n_{app} values, indicate that each of processes **I**−**III** involves the transfer of one electron equivalent, consistent with Scheme 1.

The addition of 4 equiv of $HClO_4$ produces a cyclic voltammogram in which two new processes, *III* and *IV*, are observed (Figure 3; Table 4). Processes **I** and **II** remain. These four processes are also detected by RDEV (Figure 4; Table 5). Plots of i_L vs $\omega^{1/2}$ are linear for each process (Figure S7), consistent with mass transport control. The relative limiting currents i_L are **I**:**II**:*III*:*IV* = 1.0:0.93:1.96:1.8 (N_r, 2000 min^{-1}), indicating that processes *III* and *IV* are overall $2e^-$ processes. However, the ΔE_p (Table 4) and n_{app} (Table 5) values demonstrate clearly that these are not simple $2e^-$ processes in which electrons transfer simultaneously at a single potential. For such processes,

(30) Insolubility of the $2e^-$ reduced salt $[Bu_4N]_6[S_2W_{18}O_{62}]$ is unlikely to be the cause as the CV experiments were unaffected (Figure S2).
(31) Deviations from ideal behavior ($n_{app} \sim 0.90(5)$) are again consistent with the presence of uncompensated resistance in the cell.

Table 4. Cyclic Voltammetry Data for $[Bu_4N]_4[S_2W_{18}O_{62}]$ (1.0×10^{-3} M) in MeCN/H_2O (95/5 v/v; Bu_4NClO_4, 0.1 M; $HClO_4$, 4.0×10^{-3} M)

ν (V s^{-1})	$E_{1/2}$ (V)	E_{pc} (V)	ΔE_p (V)	i_{pc} (μA mM^{-1})	$i_{pc}\nu^{-1/2}$ (μA $s^{1/2}$ $V^{-1/2}$)	$\lvert i_{pa}/i_{pc}\rvert$
			III			
0.020	−0.710	−0.735	0.055	−13.2	−3.0	1.1
0.050	−0.710	−0.740	0.060	−19.8	−2.8	1.1
0.100	−0.710	−0.745	0.070	−26.8	−2.7	1.2
0.200	−0.715	−0.755	0.080	−37.8	−2.7	1.2
0.500	−0.715	−0.770	0.105	−57.7	−2.6	1.3
1.000	−0.720	−0.785	0.140	−79.3	−2.5	1.3
			IV			
0.020	−0.960	−0.990	0.060	−11.9	−2.7	1.1
0.050	−0.960	−0.995	0.065	−16.8	−2.4	1.2
0.100	−0.960	−0.995	0.070	−23.6	−2.4	1.2
0.200	−0.960	−1.000	0.075	−33.4	−2.4	1.2
0.500	−0.965	−1.015	0.095	−52.1	−2.3	1.2
1.000	−0.970	−1.035	0.125	−70.8	−2.2	1.3

Table 5. Rotating Disk Electrode Voltammetry Data[a] for $[Bu_4N]_4[S_2W_{18}O_{62}]$ (1.0×10^{-3} M) in MeCN/H_2O (95/5 v/v; Bu_4NClO_4, 0.1 M; $HClO_4$, 4.0×10^{-3} M)

rotation rate		process *III*			process *IV*		
N_r (min^{-1})	ω (s^{-1})	$E_{1/2}$ (V)	i_L (μA)	n_{app} [a]	$E_{1/2}$ (V)	i_L (μA)	n_{app} [b]
500	52.4	−0.720	−44.5	1.27	−0.980	−42.1	1.11
1000	104.7	−0.730	−63.3	1.22	−0.990	−60.8	1.11
1500	157.1	−0.735	−78.2	1.20	−0.990	−73.3	1.19
2000	209.4	−0.735	−90.4	1.16	−1.000	−82.8	1.03
2500	261.8	−0.740	−100.9	1.11	−1.015	−103.1	0.87
3000	314.16	−0.740	−109.2	1.10	−1.010	−108.9	1.17

[a] ν, 0.1 V s^{-1}. [b] Based upon the assumption of a single ne^- process (see text).

ΔE_p would be 56/2 = 28 mV and n_{app} would be 2.0. The data are consistent with two $1e^-$ transfer processes, occurring at different potentials, with associated proton-transfer reactions.

Coupled electron/proton transfer is typical of polyoxo anion systems in which effective coalescence of pairs of $1e^-$ processes occurs to produce apparent $2e^-$ processes, driven by protonation of reduced products as a consequence of their higher basicity.[17,32−37] Apparently, processes **III** and **IV** have transformed into process *III*, and a pair of processes (**V** and **VI**) at more negative potentials have coalesced to process *IV*. An approach to analysis of such complex systems has been recently developed.[20] It involves the simulation of cyclic voltammograms, as a function of acid concentration, progressing systematically to conditions of increasing voltammetric complexity.

Figure 5 documents the behavior of $[Bu_4N]_4[S_2W_{18}O_{62}]$ (1×10^{-3} M) in MeCN/H_2O (95/5, v/v; 0.1 M Bu_4NClO_4) as a function of $HClO_4$ concentration in the range 0.25−1 equiv. Process **IV** initially loses current intensity, as new process *III* grows in at a potential between processes **II** and **III**. Process **III** also loses current intensity as the acid concentration increases. At 1 equiv of acid (Figure 5c), the development of *III* is dominating the voltammogram, and at 4 equiv (Figure 3), both *III* and *IV* are fully developed.

For process *III* to grow in between processes **II** and **III** (Figure 5) as observed, the $2e^-$ reduced anion $[S_2W_{18}O_{62}]^{6-}$, the product of **II**, must protonate. Scheme 2 was proposed for the simulation on the basis of the relative anionic charge being the major determinant of basicity in these polyoxo anion systems.[18,20] All species of anionic charge more negative than 6− are involved in protonic equilibria.

(32) Wu H. *J. Biol. Chem.* **1920**, *43*, 189.
(33) Pope, M. T.; Varga G. M. *Inorg. Chem.* **1966**, *5*, 1249.
(34) Pope, M. T.; Papaconstantinou, E. *Inorg. Chem.* **1967**, *6*, 1147.
(35) Tourné, C. *Bull. Soc. Chim. Fr.* **1967**, 3196, 3199, 3214.
(36) Contant, R.; Fruchart, J.-M. *Rev. Chim. Miner.* **1974**, *11*, 123.
(37) Keita, B.; Nadjo, L. *J. Electroanal. Chem.* **1987**, *227*, 77.

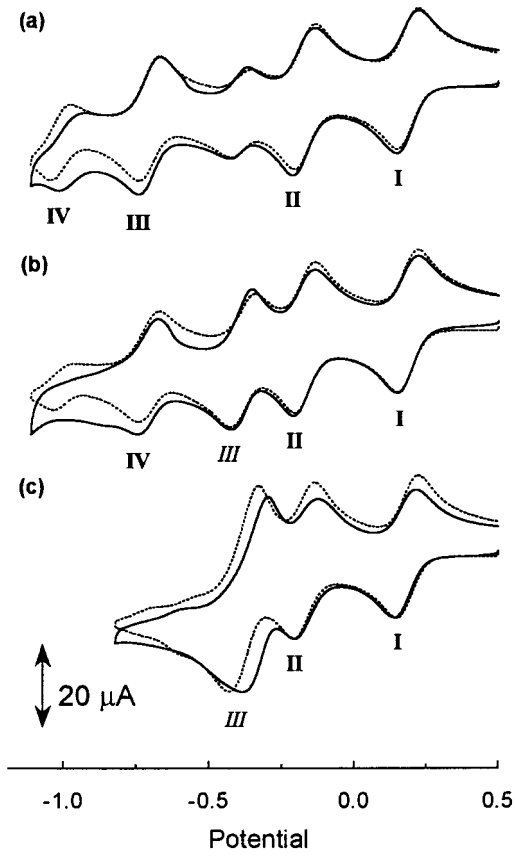

Figure 5. Experimental (—) and simulated (- - -) cyclic voltammograms for $[Bu_4N]_4[S_2W_{18}O_{62}]$ (9.7×10^{-4} M) in MeCN (0.1 M Bu_4NClO_4); ν, 0.100 V s^{-1}. Mole equivalents of $HClO_4$: (a) 0.25, (b) 0.50, (c) 1.00.

Scheme 2

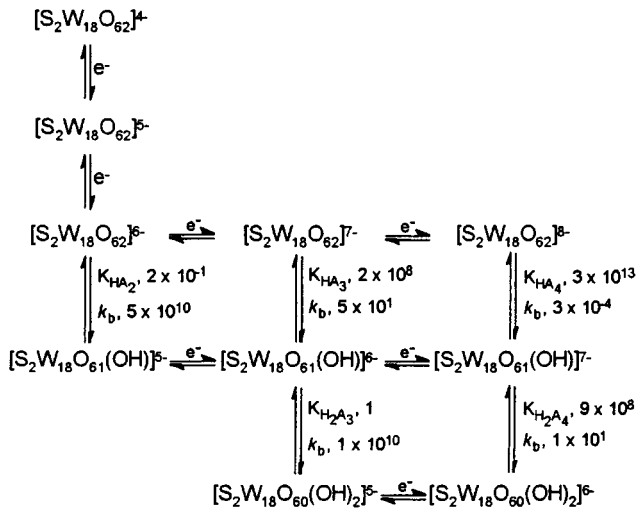

Background parameters for the simulations are discussed in the Experimental Section. Input $E_{1/2}$ values for processes **I**−**IV** were taken from Table S2. As protonation is normally a fast process, all forward rate constants for protonation k_f were assumed to be diffusion controlled and were set to 10^{10} M^{-1} s^{-1}. The equilibrium constants, K_{HA_x} and $K_{H_2A_x}$ ($x = 2-4$), were varied to yield the best fit, and thus determine the back rate constants according to $K_{HA_x} = k_{fx}/k_{bx}$. The systematic approach to simulation outlined in ref 20 was adopted, leading to the fits shown in Figure 5. Optimization of the diffusion coefficient for H^+ led to a final value of 1.5×10^{-5} cm^2 s^{-1}. This diffusion coefficient value can be compared with 1.8×10^{-5} cm^2 s^{-1}, obtained for the $[S_2Mo_{18}O_{62}]^{4-}$ system.[18] As expected for diffusion-controlled processes, inclusion of disproportionation (cross) reactions resulted in no improvement to the fits. Derived parameters are listed in Table 6. The validity of the parameters was established by using them to predict behavior as a function of anion concentration.[20] For example, the parameters provided acceptable fits for data collected at 1.5 times the concentration of Figure 5 (Figure S8).

Table 6. Parameters for Simulation of Cyclic Voltammetry of $[Bu_4N]_4[S_2W_{18}O_{62}]$ (9.7×10^{-4} M) in MeCN (Bu_4NClO_4, 0.1 M; ν, 0.100 V s^{-1})

Redox Couples	$E_{1/2}$ [a] (V)
$[S_2W_{18}O_{62}]^{4-} \overset{e^-}{\rightleftharpoons} [S_2W_{18}O_{62}]^{5-}$	−0.23
$[S_2W_{18}O_{62}]^{5-} \overset{e^-}{\rightleftharpoons} [S_2W_{18}O_{62}]^{6-}$	−0.59
$[S_2W_{18}O_{62}]^{6-} \overset{e^-}{\rightleftharpoons} [S_2W_{18}O_{62}]^{7-}$	−1.12
$[S_2W_{18}O_{62}]^{7-} \overset{e^-}{\rightleftharpoons} [S_2W_{18}O_{62}]^{8-}$	−1.43
$[S_2W_{18}O_{61}(OH)]^{5-} \overset{e^-}{\rightleftharpoons} [S_2W_{18}O_{61}(OH)]^{6-}$	−0.59
$[S_2W_{18}O_{61}(OH)]^{6-} \overset{e^-}{\rightleftharpoons} [S_2W_{18}O_{61}(OH)]^{7-}$	−1.12
$[S_2W_{18}O_{60}(OH)_2]^{5-} \overset{e^-}{\rightleftharpoons} [S_2W_{18}O_{60}(OH)_2]^{6-}$	−0.59
Protonic Equilibria	K_{eq} (M^{-1})
$[S_2W_{18}O_{62}]^{6-} \overset{H^+}{\rightleftharpoons} [S_2W_{18}O_{61}(OH)]^{5-}$	K_{HA_2}, 2×10^{-1}
$[S_2W_{18}O_{62}]^{7-} \overset{H^+}{\rightleftharpoons} [S_2W_{18}O_{61}(OH)]^{6-}$	K_{HA_3}, 2×10^{8}
$[S_2W_{18}O_{62}]^{8-} \overset{H^+}{\rightleftharpoons} [S_2W_{18}O_{61}(OH)]^{7-}$	K_{HA_4}, 3×10^{13}
$[S_2W_{18}O_{61}(OH)]^{6-} \overset{H^+}{\rightleftharpoons} [S_2W_{18}O_{60}(OH)_2]^{5-}$	$K_{H_2A_3}$, 1
$[S_2W_{18}O_{61}(OH)]^{7-} \overset{H^+}{\rightleftharpoons} [S_2W_{18}O_{60}(OH)_2]^{6-}$	$K_{H_2A_4}$, 9×10^{8}

Nevertheless, as with all simulations of complex reaction schemes, some caution must be attached to the outcome; the solution presented may not be unique, and the significance of each parameter is not necessarily equivalent in a statistical sense. However, despite this limitation, the simulation appears to provide a realistic evaluation of the trends underpinning the complex electron- and proton-transfer reactions. Thus, estimated $E_{1/2}$ values for anions with the same overall anionic charge are approximately the same as would be expected from charge considerations. For example, derived values for couples $[S_2W_{18}O_{62}]^{6-/7-}$ and $[S_2W_{18}O_{61}(OH)]^{6-/7-}$ are each −0.70 V, while those for $[S_2W_{18}O_{62}]^{5-/6-}$, $[S_2W_{18}O_{61}(OH)]^{5-/6-}$, and $[S_2W_{18}O_{60}(OH)_2]^{5-/6-}$ are −0.17 V. Protonation constants also depend on the anionic charge. For $[S_2W_{18}O_{62}]^{n-}$ ($n = 6-8$), K_H increases from 2×10^{-1} to 2×10^{8} to 3×10^{13} M^{-1} (Scheme 2; Table 6). In addition, values are similar for the pairs $\{[S_2W_{18}O_{62}]^{6-}, [S_2W_{18}O_{61}(OH)]^{6-}\}$ and $\{[S_2W_{18}O_{62}]^{7-}, [S_2W_{18}O_{61}(OH)]^{7-}\}$.

Interestingly, the equilibrium constant for protonation of the $2e^-$ reduction product $[S_2W_{18}O_{62}]^{6-}$ (K_{HA_2}, 2×10^{-1} M^{-1}; Scheme 2; Table 6) is small and might be expected to have a minor effect on the outcome of the simulation. However, this reaction appears to be key in understanding the fundamental mechanism of electron transfer. Its omission led to large deviations between the simulated and experimental voltammograms, mainly by the simulation predicting chemical irreversibility of processes at more negative potentials. As this is not observed experimentally, protonation of the $2e^-$ reduction product, $[S_2W_{18}O_{62}]^{6-}$, appears to be important as a pathway for the back reactions (oxidation, deprotonation) involving the more reduced species.

As discussed above, the protonation constants increase by multiple orders of magnitude as the overall charge on the anions increases (Table 6). The crucial assumption that all protonation rates k_f are large (10^{10} M^{-1} s^{-1}) means that the deprotonation rates k_b follow the opposite order of the protonation constants

Scheme 3

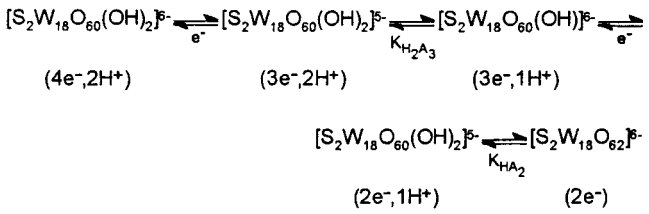

Scheme 4

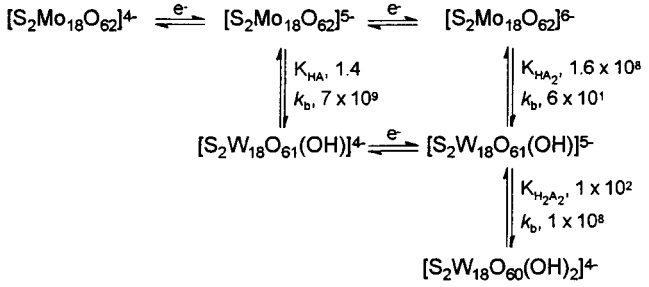

$K_H = k_f/k_b$ (Scheme 2). Consequently, the experimentally observed reversibility of the voltammetry is a result of:

(i) multiple reduction/protonation pathways being possible, as parameters k_f are large;[38]

(ii) the only viable oxidation pathway being via equilibria $K_{H_2A_3}$ and K_{HA_2}, as parameters k_b are large for this pathway only (Schemes 2 and 3).

Thus, the inclusion of protonation equilibrium K_{HA_2} involving the 2e$^-$ reduced anion $[S_2W_{18}O_{62}]^{6-}$ (the product of process**II**) is essential as it is part of the only pathway for rapid oxidation.

The key observations for this $[S_2W_{18}O_{62}]^{4-}$ system in MeCN/H_2O differ from those seen for the molybdenum anion $[S_2Mo_{18}O_{62}]^{4-}$. In the latter system, the behavior was consistent with rapid protonation following formation of the 1e$^-$ reduced anion $[S_2Mo_{18}O_{62}]^{5-}$ (the product of process **I**, Scheme 4).[18] A similar fast reoxidation pathway exists (Scheme 4). However, comparison of the reduction/protonation schemes for the tungsten and molybdenum systems (Schemes 2 and 4, respectively) indicates a difference in intrinsic basicity. In the molybdenum system, the 1e$^-$ redox level is the first to be able to provide a high rate constant k_b for the final deprotonation step (via K_{HA}, Scheme 4). In the tungsten system, the 2e$^-$ redox level is the first to exhibit this property (Scheme 2).

The outer-layer oxygen atoms in heteropoly complexes are strongly polarized toward the interior of the molecule, causing the oxo ligands to be relatively positive in character and the fully oxidized anions to be weak bases.[39] W(VI) appears to be more electropositive than Mo(VI),[40] and so at a given redox level, the tungsten polyoxo anion will be less basic than its molybdenum analogue. This provides a preliminary rationalization for the observation that, under equivalent conditions, initial coalescence of 1e$^-$ processes occurs at the $[S_2Mo_{18}O_{62}]^{4-/5-/6-}$ couples (Scheme 4[18]) and at the $[S_2W_{18}O_{62}]^{6-/7-/8-}$ couples (Scheme 2), respectively. It is assumed that the influence of the differences in structure between $[S_2Mo_{18}O_{62}]^{4-}$ and $[S_2W_{18}O_{62}]^{4-}$ is secondary to the electronegativity effects.

The spectacular increase in protonation constants with anionic charge in these series may be associated with localization of electron density in the belts of reduced Dawson anions.[15,41−45] There is now direct structural evidence of this phenomenon in the series of α-anions $[S_2Mo_{18}O_{62}]^{4-}$ (oxidized), $[HS_2Mo_{18}O_{62}]^{5-}$ (reduced by 2e$^-$, 1 H$^+$), and $[H_3S_2Mo_{18}O_{62}]^{5-}$ (reduced by 4 e$^-$, 3 H$^+$).[46,47] As two and then four electrons are added, the average Mo···Mo distance across the belts decreases (see structure I). In the polyoxometalate systems studied here, simulation predicts that K_{HA_x} values increase by 10^4-10^9 for a unit increase of overall anionic charge (Table 6; see also refs 18 and 20). These are large increases, particularly for clusters with high surface areas. There is a similar spectacular "anomoly" associated with large increases in experimental $E_{1/2}$ values under *aprotic* conditions. For example, increases by 0.4−0.6 V for the reduction of $[S_2W_{18}O_{62}]^{n-}$ are seen for $n = 4-7$ (Table 6). These phenomena are related in that it is apparent that the system is responding to differences in anionic charge. However, it is probable that the anionic charge is not distributed uniformally on the surface, and the exact protonation sites remain unidentified.

Finally, it can be noted that the reversible potentials for the reduction of the $[S_2W_{18}O_{62}]^{4-}$ system are significantly more negative than those found for the $[S_2Mo_{18}O_{62}]^{4-}$ system. This is the same order as found for $[MF_6]^{0/-}$ (M = Mo, W) where the processses are fully metal-based.[48,49] In the polyoxometalate case, the added electron is delocalized over a framework so that a smaller difference in $E_{1/2}$ values is expected and is observed.

Summary

The synthesis and structure of the γ*-$[S_2W_{18}O_{62}]^{4-}$ anion are presented, together with a detailed examination of its electrochemistry. In MeCN solution, $[S_2W_{18}O_{62}]^{4-}$ undergoes four reversible 1e$^-$ reduction processes. Addition of 4 equiv of $HClO_4$ to MeCN/H_2O solutions causes the two most cathodic of these processes to coalesce into a 2e$^-$ process. Computer simulation of this behavior provides insights into the redox and protonation equilibria that are responsible for the complex behavior. In particular, while multiple pathways for correlated reduction and protonation are observed, only a single fast oxidation pathway is available. This is postulated to be the origin of the highly reversible electrochemical behavior, characteristic of polyoxometalate anions in acidic media in general.

Acknowledgment. A.G.W. and A.M.B. thank the Australian Research Council for support via Grants A29531579 and A294801726.

Supporting Information Available: Table S1−S3 and Figures S1−S5 showing RDEV data. An X-ray crystallographic file for $[Bu_4N]_4[S_2W_{18}O_{62}]\cdot 1.23MeCN\cdot 0.27H_2O$ in CIF format. This material is available free of charge via the Internet at http://pubs.acs.org.

IC000793Q

(38) Note that access to the (4e$^-$, 2H$^+$)-reduced level is possible via equilibria $K_{H_2A_3}$ and K_{HA_2} (reverse of Scheme 3) by holding the potential at the $E_{1/2}$ value of **II** (−0.62 V). The $E_{1/2}$ values of the intermediate redox levels are also about −0.62 V (Table 6).

(39) Baker, L. C. W.; Glick, D. C. *Chem. Rev.* **1998**, *98*, 3.
(40) Huhey, J. E.; Keiter, E. A.; Keiter, R. L. *Inorganic Chemistry*, 4th ed.; Harper-Collins: New York, 1993; pp 189−190.
(41) Prados, R. A.; Pope, M. T. *Inorg. Chem.* **1976**, *15*, 2547.
(42) Kazanskii, L. P.; Fedotov, M. A. *J. Chem. Soc., Chem. Commun.* **1980**, 644.
(43) Barrows, J. N.; Pope, M. T. *Inorg. Chim. Acta* **1993**, *213*, 91.
(44) Kozik, M.; Hammer, C. F.; Baker, L. C. W. *J. Am. Chem. Soc.* **1986**, *108*, 2748.
(45) Casan-Pastor, N.; Baker, L. C. W. *J. Am. Chem. Soc.* **1992**, *114*, 10384.
(46) Neier, R.; Trojanowski, C.; Mattes, R. *J. Chem. Soc., Dalton Trans.* **1995**, 2521−2828.
(47) Juraja, S.; Vu, T.; Richardt, P. J. S.; Bond, A. M.; Cardwell, T. J.; Cashion, J. D.; Fallon, G.; Lazarev, G.; Moubaraki, B.; Murray, K. S.; Wedd, A. G., submitted for publication.
(48) Bond, A. M.; Irvine, I.; O'Donnell, T. A. *Inorg. Chem.* **1975**, *14*, 2408; **1977**, *16*, 841.
(49) Brownstein, S.; Heath, G. A.; Sengupta, A.; Sharp, D. W. A. *J. Chem. Soc., Chem. Commun.* **1983**, 669.